



Impact of Atmospheric Turbulence on Dynamic Wind Loads on Heliostats

Azadeh Jafari¹ , Matthew J. Emes¹ , and Maziar Arjomandi¹ 

¹ School of Electrical and Mechanical Engineering, University of Adelaide

* Correspondence: Azadeh Jafari, azadeh.jafari@adelaide.edu.au

Abstract. This study analyses the turbulent wind properties in the lower 10 m of the atmospheric surface layer close to the ground where heliostats are located. Power spectral densities of streamwise and vertical components of wind are analysed, and the frequencies associated with the peak of the spectra are determined using field data collected at two open-country terrains in addition to spectral models of ESDU85020. Variations of the peak frequencies with height from the ground, terrain type and average wind speed are discussed and the impact on heliostat wind loads are described. It is found that while the peak frequency of the streamwise turbulence is between 0.01–0.1 Hz, the peak of the vertical turbulence occurs at frequencies in the range of 0.1–1 Hz. It is shown that smaller heliostats that are located closer to the ground are exposed to turbulent wind fluctuations at a higher frequency and are thus expected to experience wind loads with a higher dominant frequency compared to larger heliostats located higher above the ground. These frequencies need to be considered in design of heliostat drives and structural components.

Keywords: Turbulence, Wind Loads, Heliostats.

1. Introduction

Wind loading is an important consideration in the design of the support structures and drives of a heliostat accounting for up to 80% of the capital cost of a heliostat [1]. The wind loads on heliostats are highly impacted by the turbulent properties in the lower 10 m of the atmospheric surface layer (ASL) close to the ground. The ASL consists of a series of turbulent structures of various length scales and frequencies, which create fluctuations in wind speed through continuous energy exchange with one another and with the bulk flow. Previous studies have shown that the mean and peak wind loads on heliostats are strongly impacted by intensity and length scales of wind turbulence [2-6]. The dynamic time-variations of wind loads and the impact of wind turbulence on those are yet not well characterised.

The dynamic loads on heliostats are induced by the correlation between the temporal variations of the wind loads and the dynamic properties of the heliostat structure. Dynamic loads may lead to vibrations of the heliostat panel which impact the tracking accuracy of the heliostat field and consequently the optical efficiency of the solar plant. Moreover, assessment of the dynamic response of the heliostats under unsteady wind loads is important for preventing dynamic failure arising from resonance and buffeting [7], which may result when the peak frequencies of the wind loads are close to the natural frequencies of the heliostat structures, which typically lie in the range of 1–10 Hz [8-10].

This study presents an analysis of the power spectral density (PSD) of turbulent wind velocity fluctuations in the ASL and its impact on the dynamic loads on full-scale heliostats. Atmospheric field data collected near the ground and at heights below 12 m at two open-country terrains are analysed and the frequencies associated with the peaks of streamwise and vertical turbulence spectra are determined. Additionally, wind models of ESDU85020 [11] are employed to evaluate the effect of terrain roughness and average wind speed on the peak frequencies of wind turbulence. The ASL data and analysis are presented in Section 3 and their impact on heliostat wind loads is discussed in Section 4.

2. Methodology

The wind PSD describes the distribution of the energy of the turbulent wind fluctuations with their frequency. PSD is calculated from the Fast Fourier Transform of the fluctuating component of the measured wind velocity time series using the *pwelch*-function in MATLAB. The PSDs of horizontal and vertical wind velocity fluctuations are analysed using two sets of data from field measurements of ASL and an empirically developed model. The first dataset was collected at the Atmospheric Boundary Layer Research Facility (ABLRF) at the University of Adelaide Roseworthy campus [12, 13]. Wind velocities were measured using five 81005A RM Young three-dimensional ultrasonic anemometers positioned on a 12m lattice tower with logarithmical spacing at heights of 1.6 m, 3.1 m, 4.6 m, 7.9 m, and 12 m. The measurements were conducted during one hour on 14 January 2023 with an hourly south-western mean wind direction (223°) at a sampling frequency of 32 Hz. The streamwise (u) and vertical (w) components of instantaneous velocity were obtained after correcting for the mean wind speed directions and the PSDs were calculated (shown in Figure 1 at heights of 3.1 m and 12 m). The mean wind velocity profile of the ABLRF site is shown to be consistent with a flat, open-country terrain, with a surface roughness height $z_0 = 0.03$ m [12, 13]. The second analysis was conducted based on the published near-neutral atmospheric measurements from the Cooperative Atmosphere Surface Exchange Study field campaign of 1999 (CASES-99) [14, 15]. The topography of the site was flat with shallow gullies and very gentle slopes covered with grass and was characterised to represent an open-country terrain with a surface roughness height of $z_0 = 0.04$ m [15]. Finally, the ASL spectra are estimated from the PSD equations given by ESDU85020 [11] which provide a modified version of Von Karman's model, expressing the power spectral density of streamwise and vertical velocity components for terrains with different surface roughness and variable mean wind speeds.

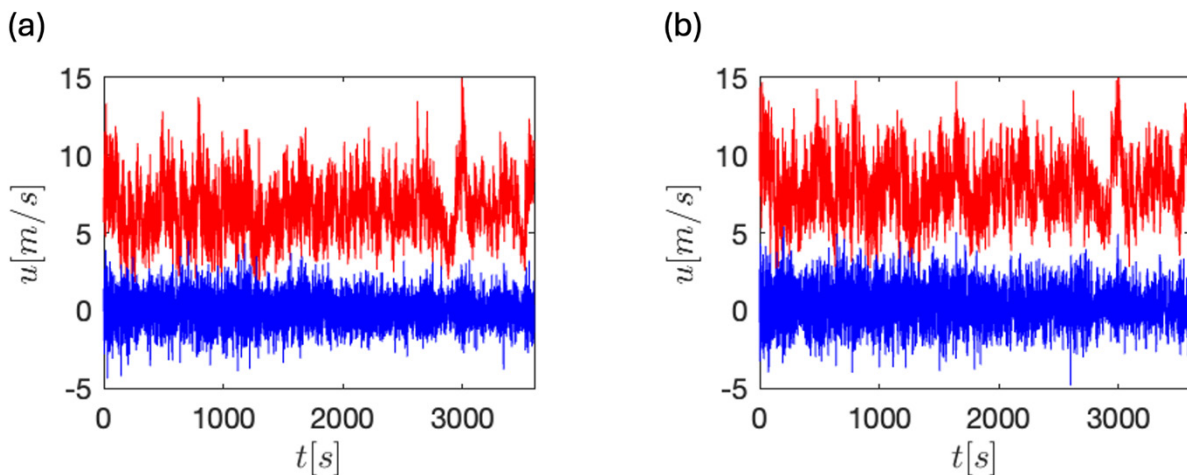


Figure 1. Time series of instantaneous wind velocity at ABLRF on 14 Jan 2023: (a) $z = 3.1$ m, and (b) $z = 12$ m. The streamwise and vertical velocity components are shown in red and blue, respectively.

3. Analysis of wind turbulence spectra in near-surface ASL

3.1. Streamwise and vertical PSDs at ABLRF

Figure 2 shows the PSD of streamwise and vertical components of wind velocity fluctuations at different heights at ABLRF. The estimations from ESDU model for the same terrain roughness and average wind speed ($z_0 = 0.03$ m and $U_{10} = 8$ m/s) are also shown in dashed and solid black lines. Comparison of the profiles shows a good overall agreement between the field measurements and the ESDU model with a shift to higher peak frequencies in the field measurements particularly for the vertical velocity. Based on the ABLRF measurements the peak frequency of the streamwise turbulence is between ~ 0.01 – 0.02 Hz, while the peak of the vertical turbulence occurs at frequencies in the range of ~ 0.2 – 1 Hz. The results show that the vertical velocity fluctuations are at higher frequencies compared to streamwise velocity fluctuations at the same height. For example, at $z=3$ m, the peak of the streamwise turbulence spectrum occurs at an approximate frequency of 0.015 Hz while the peak of vertical turbulence spectrum is at an approximate frequency of 0.48 Hz. The larger frequencies of the vertical velocity fluctuations are due to the anisotropy of turbulence [15, 16]. In the near-neutral ASL, the turbulence structures near the ground have larger length scales in the streamwise direction compared to the vertical direction and thus the frequencies of streamwise turbulence are lower compared to vertical turbulence.

3.2. Peak frequencies of turbulence at different heights

The frequencies at which the peak of the turbulence spectra for streamwise and vertical velocity components occur at different heights are plotted in Figure 3(a) and Figure 3(b) from the PSDs of ABLRF and CASES99 data and their corresponding ESDU estimations. The observations at both ABLRF and CASES-99 show that the frequencies of the peaks of vertical turbulence spectra are larger than the peaks of the streamwise turbulence at similar heights. It is also shown that at lower heights closer to the ground, both the velocity fluctuations shift to higher frequencies. For example, at ABLRF (Figure 3(a)), the frequency of the peak of vertical turbulence spectrum shifts from ~ 0.17 Hz at $z=12$ m to ~ 0.85 Hz at $z=1.6$ m. The peak frequencies from the CASES-99 (Figure 3(b)) measurements are in general higher than the ESDU predictions at the same heights but show a similar trend and increase at lower heights closer to the ground. The peak of streamwise turbulence increases from ~ 0.03 Hz at $z=10$ m to ~ 0.12 Hz at $z=1.5$ m. Similarly, the peak of vertical turbulence shifts from ~ 0.3 Hz at $z=10$ m to ~ 0.56 Hz at $z=1.5$ m. The increase of peak frequencies closer to the ground is due to the scaling of turbulent structures in the near-neutral ASL with height from the ground. As discussed by [16], in the near-neutral ASL (at heights from the order of millimetres to the order of 100 m), the turbulent structures grow in length scales with increase of height above the ground (in accordance with Townsend's attached-eddy hypothesis for a turbulent boundary layer).

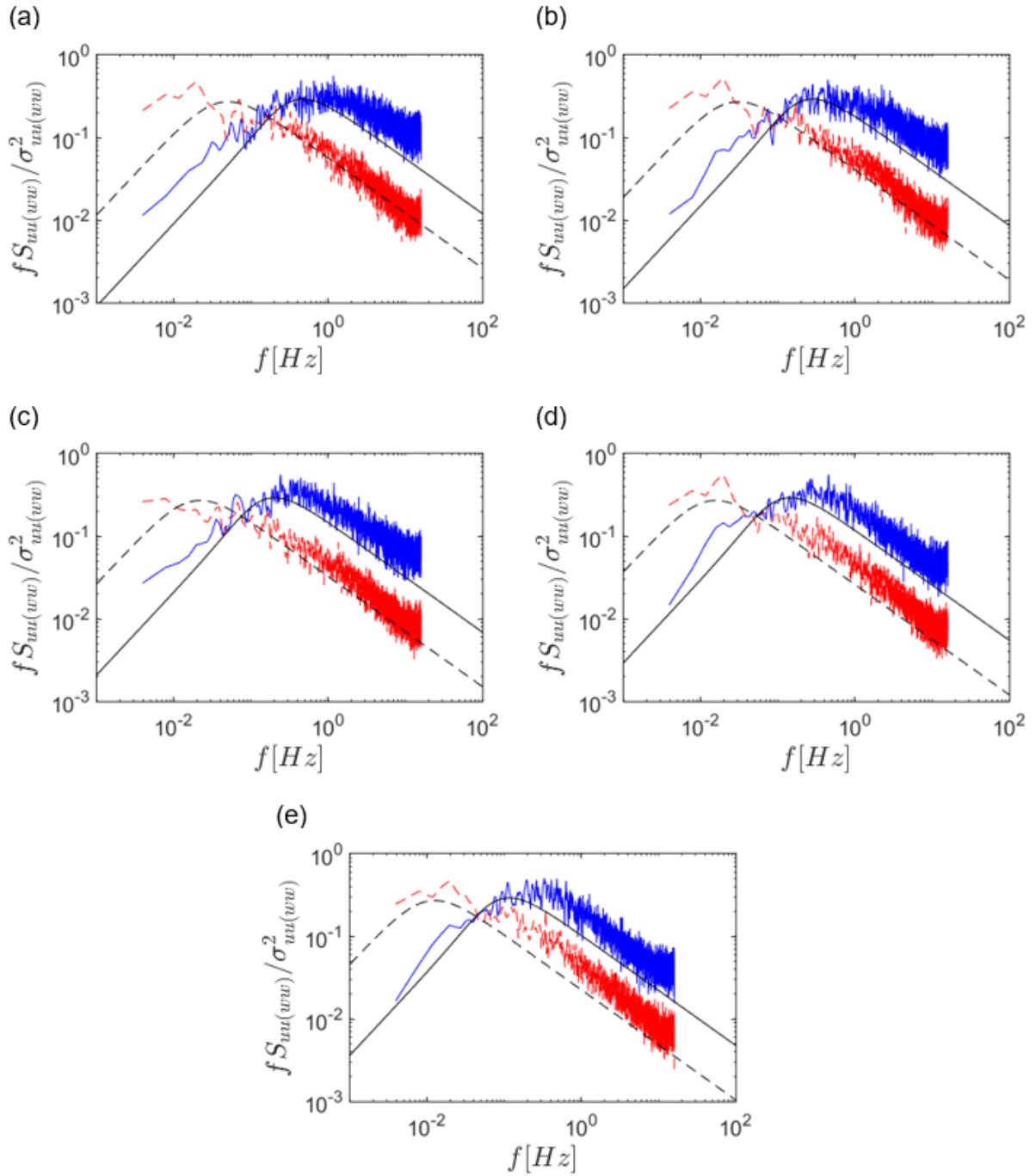


Figure 2. Normalised PSDs (f, S, σ show frequency, power spectral density and standard deviation of velocity fluctuations, respectively) of streamwise (dashed red) and vertical (solid blue) fluctuating velocity components from measurements at ABLRF on 14 Jan 2023. The dashed and solid black lines show the estimated streamwise and vertical velocity PSDs using the ESDU85020 [11] model for a similar terrain and average wind speed ($z_0 = 0.03$ m, $U_{10} = 10$ m/s). (a) $z = 1.6$ m, (b) $z = 3.1$ m, (c) $z = 4.6$ m, (d) $z = 7.9$ m, and (e) $z = 12$ m.

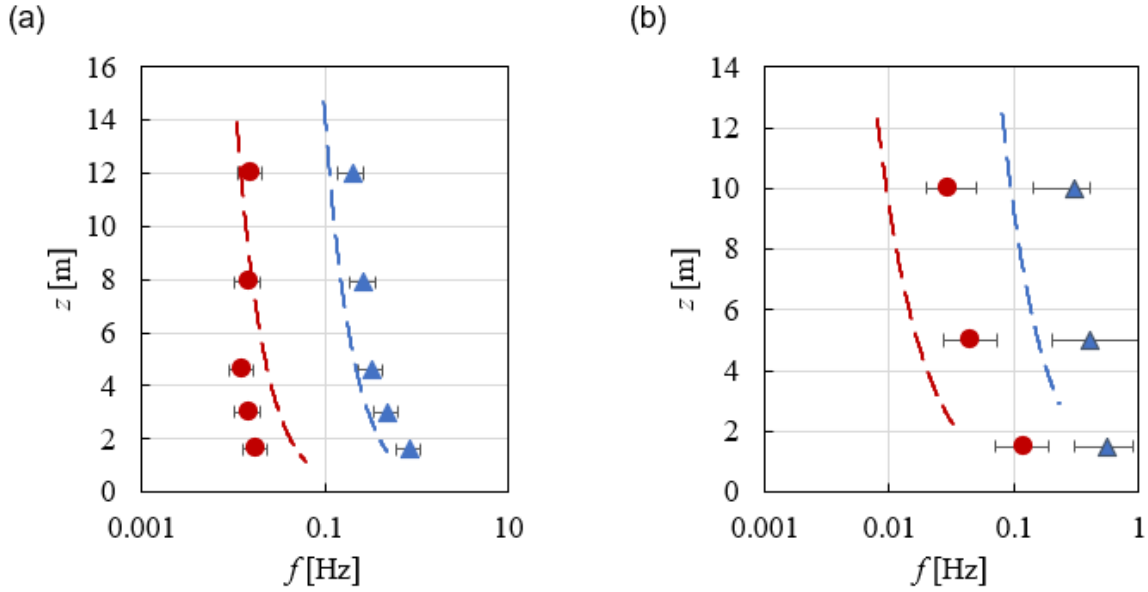


Figure 3. The peak frequencies of wind turbulence at different heights from the ground: (a) ABLRF, (b) CASES99. The red and blue colours refer to streamwise and vertical velocities. Dashed lines show the peak frequencies estimated from ESDU85020 [11] for similar terrain and average wind speeds ($z_0 = 0.03$ m, $U_{10} = 10$ m/s for ABLRF and $z_0 = 0.04$ m and $U_{10} = 5$ m/s for CASES99).

3.3. Effect of terrain type on the peak frequency of turbulence

Turbulence in the atmospheric flow is dependent on the features of the surrounding terrain and varies based on the site of different heliostat fields. The terrain is often characterised by its surface roughness which is between $z_0 = 0.001$ – 0.003 m for a flat terrain, $z_0 = 0.01$ – 0.03 m for an open-country terrain, and $z_0 = 0.1$ – 0.3 m for a suburban terrain, based on ESDU85020 [11]. To investigate the effect of terrain type on the peak frequencies of streamwise and vertical turbulence spectra in the lower ASL, the PSDs of both velocity components were calculated for different surface roughness values using the ESDU model and the frequencies corresponding to the peak of the spectra were determined similarly to the results of the previous section. Figure 4(a) shows the peak frequencies of streamwise and vertical wind velocity fluctuations for $z_0 = 0.001, 0.01, 0.1$ m at different heights from the ground between 3 m and 10 m. For all different terrain types, the peak frequencies increase with decrease of height closer to the ground. Furthermore, terrains with a larger surface roughness have slightly higher peak frequencies at lower heights closer to the ground. For example, at $z=3$ m, with increase of surface roughness from $z_0 = 0.001$ m to $z_0 = 0.1$ m, a flat terrain to a suburban terrain, peak of the vertical turbulence increases from ~ 0.23 Hz to ~ 0.27 Hz. Similarly, the peak of streamwise velocity fluctuations increases from ~ 0.02 Hz to ~ 0.03 Hz. The effect of terrain roughness on the peak frequencies however becomes less with increase of height from the ground. Therefore, at height closer to the ground, change of a terrain to a rougher type increases the peak frequencies while the peak of vertical turbulence remains almost one order of magnitude larger than the peak of streamwise turbulence.

3.4. Effect of average wind speed on the peak frequency of turbulence

Figure 4(b) shows the effect of average wind speed U_{10} (wind speed at $z=10$ m) on the peak frequencies of streamwise and vertical wind velocity fluctuations at different heights from the ground between 3 m and 10 m. It is shown that with increase of the mean wind speed, the peak frequencies of both streamwise and vertical turbulence increase at all heights from the ground. For example, with increase of U_{10} from 5 m/s to 20 m/s, the peak of streamwise velocity fluctuations increases from ~ 0.02 Hz to ~ 0.07 Hz at $z=3$ m and from ~ 0.01 Hz to ~ 0.02 Hz at $z=10$ m. Similarly, the peak of vertical velocity fluctuations increases from ~ 0.2 Hz to ~ 0.6 Hz

at $z=3$ m and from ~ 0.1 Hz to ~ 0.2 Hz at $z=10$ m. For all heights and average wind speeds, the peak of vertical turbulence remains one order of magnitude larger than the peak of streamwise turbulence. For example, at $z=3$ m, the peak of vertical turbulence is at ~ 0.6 Hz as compared to ~ 0.07 Hz for streamwise turbulence at $U_{10} = 20$ m/s. It is also shown in Figure 4(b) that considering mean wind speeds of $U_{10} = 5\text{--}20$ m/s and at heights below 10 m, the peak frequency of the streamwise turbulence is between $\sim 0.01\text{--}0.1$ Hz, and the peak of the vertical turbulence occurs at frequencies in the range of $\sim 0.1\text{--}1$ Hz.

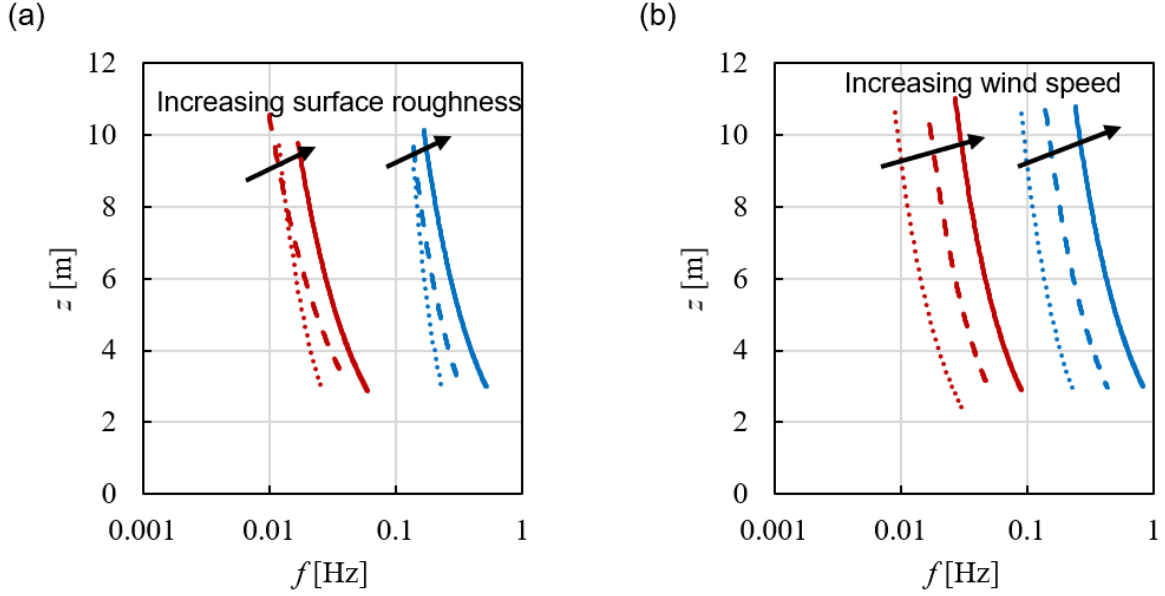


Figure 4. Peak frequencies of streamwise and vertical wind turbulence at different heights from the ground based on ESDU85020 model for: (a) different surface roughness values ($z_0 = 0.001, 0.01, 0.1$ m) at $U_{10} = 10$ m/s, (b) different average wind speeds (at $U_{10} = 5, 10, 20$ m/s) at $z_0 = 0.01$ m. The red and blue colours correspond to streamwise and vertical velocities, respectively.

4. Correlation between wind spectra and dynamic wind loads on heliostats

The spectral distribution of the wind loads can be correlated with the turbulence power spectrum through the aerodynamic admittance function [17]:

$$|A_{L(D)}(f)|^2 = \frac{U^2 S_{C_{L(D)}}}{C_{L(D)}^2 S_{ww(uu)}}$$

where $A(f)$ is the aerodynamics admittance function, $S_{C_{L(D)}}$ is the PSD of lift (drag) force coefficient, $S_{ww(uu)}$ shows the PSD of vertical (streamwise) velocity fluctuations, and U and $C_{L(D)}$ are the mean velocity and lift (drag) force coefficient.

Different scales and frequencies of turbulence are not equally effective in producing forces [18]. The aerodynamic admittance represents a measure of the effectiveness of a body in extracting energy from the oncoming turbulence at different frequencies [19]. While in a quasi-steady situation the contribution of velocity fluctuations of all wavelengths is assumed equal in generation of wind loads, in reality, the frequency-dependency of the forces is expressed by the aerodynamic admittance. The aerodynamic admittance function thus correlates the PSD of velocity with the PSD of the loads on a structure. Accordingly, the aerodynamic admittance is employed here to correlate the spectral distribution of heliostat wind loads with

the atmospheric wind spectra. As described in [5, 16], the fluctuating lift force on a heliostat when the mirror panel is stowed, is strongly correlated with the vertical velocity fluctuations and the drag force when the mirror panel is perpendicular to the wind direction ($\alpha = 90^\circ$ where α is the elevation angle of the mirror panel) is correlated with the streamwise component of wind turbulence. Accordingly, it was shown that the spectrum of the fluctuating lift force on a heliostat at stow position ($\alpha = 0^\circ$) can be correlated with the spectrum of vertical wind component through the aerodynamic admittance of lift force. At $\alpha = 90^\circ$ the aerodynamic admittance correlates the power spectrum of the drag force coefficient with the power spectrum of the streamwise velocity.

The aerodynamic admittance for heliostats at $\alpha = 0^\circ$ and $\alpha = 90^\circ$ was determined in [16] using force and wind data collected from wind tunnel experiments. It was shown that while the aerodynamic admittance function is frequency dependent, for both lift and drag forces, it remained almost constant and at its peak when $\frac{fc}{U} < 1$ (where f is frequency, c is the mirror panel chord length and U is the average wind speed) and reduces consistently at higher frequencies [16]. As the larger value of aerodynamic admittance function indicates a larger correlation between the wind and load frequencies, this means that turbulent structures with reduced frequencies lower than 1 are more effective in generating the wind loads and they are the major contributor to the fluctuating wind loads on heliostats. Turbulent wind fluctuations at reduced frequencies above 1 are less spatially correlated and hence less effective in generation of loads. Based on the aerodynamic admittance functions of heliostats described above, it is concluded that a direct correlation between the spectral distribution of velocity components and lift/drag forces on heliostats exists with the peak frequencies of the wind loads expected to match the peak frequency of the wind turbulence at $\frac{fc}{U} < 1$. Therefore, the peak frequency of the lift force on heliostats at near-zero and small elevation angles is expected to be close to the peak frequency of vertical velocity component and the peak frequency of the drag force at large elevation angles is expected to be close to the peak frequency of streamwise wind velocity component for heliostat size and wind speed conditions with $\frac{fc}{U} < 1$.

5. Implications for design of heliostats

Based on the analysis of turbulent wind spectra in Section 3 and the described correlation between wind loads on heliostats and wind turbulence in Section 4, the following conclusions regarding dynamic wind loads are made:

- As the peak frequency of vertical component of wind in the lower ASL is approximately one order of magnitude larger than the peak of streamwise component, critical wind loads on full-scale heliostats when operating at near-zero and small elevation angles are impacted by turbulent wind at peak frequencies that are one order of magnitude higher compared to larger elevation angles.
- As the peak frequencies of both vertical and streamwise wind velocity components increase with decrease of height from the ground, smaller heliostats that are located closer to the ground are exposed to turbulent wind fluctuations at a higher frequency and are expected to experience wind loads with a higher peak frequency compared to larger heliostats located higher above the ground.
- Increased surface roughness, from a flat to a suburban terrain, slightly increases the peak frequencies at heights closer to the ground, while maintaining one order of magnitude higher frequencies of vertical turbulence. Therefore, for smaller heliostats that are located closer to the ground, the effect of terrain roughness on wind loads needs to be more carefully analysed and considered specifically for dynamic loads at stow and small elevation angles for which the peak frequencies will be closer to the heliostat structure natural frequency.

6. Conclusions

Based on analysis of wind turbulence spectra at different terrains, mean wind speeds and at heights below 10 m, it is shown that the peak frequencies of wind turbulence are between 0.01–0.1 Hz for streamwise and between 0.1–1 Hz for the vertical component. The peak frequency of wind loads at stow and near-zero elevation angles are thus expected to be closer to the reported heliostat natural frequencies compared to the peak frequencies of wind loads at large elevation angles. This emphasises the importance of considering dynamic loads at near-zero elevation angles in the design of heliostats. Furthermore, smaller heliostats that are located closer to the ground are exposed to turbulent wind fluctuations at a higher frequency and will experience wind loads with a higher peak frequency compared to larger heliostats located higher above the ground. These frequencies need to be considered in design of heliostat drives and structural components. This also highlights the need for field data at lower heights closer to the ground to extend available models such as ESDU at lower heights for more accurate prediction of loads on smaller heliostats.

Data availability statement

Data can be accessed upon request to the authors.

Author contributions

A.J. contributed to conceptualisation, data curation, formal analysis, methodology, visualization, and writing (original draft). M.J.E. contributed to data curation and writing (review and editing). M.A. contributed to conceptualization, funding acquisition and writing (review and editing).

Competing interests

The authors declare that they have no competing interests.

Acknowledgement

The authors would like to acknowledge the financial support by HelioCon, Department of Energy (DOE) Solar Energy Technologies Office Award DE-265 EE00038488/38714 and Australian Solar Thermal Research Institute (ASTRI) by Australian Renewable Energy Agency (ARENA) Grant 1-SRI002.

References

1. G.J. Kolb, Ho, C.K., Mancini, T.R., and Gary, J.A., Power tower technology roadmap and cost reduction plan. SAND2011-2419, Sandia National Laboratories, 2011.
2. M.J. Emes, A. Jafari, A. Pfahl, J. Coventry, and M. Arjomandi, A review of static and dynamic heliostat wind loads. *Solar Energy*, 2021. 225: p. 60-82. doi: <https://doi.org/10.1016/j.solener.2021.07.014>
3. M. J. Emes, M. Arjomandi, F. Ghanadi, and R. M. Kelso, Effect of turbulence characteristics in the atmospheric surface layer on the peak wind loads on heliostats in stow position. *Solar Energy* 2017. 157: p. 284-297. doi: <https://doi.org/10.1016/j.solener.2017.08.031>
4. M. J. Emes, A. Jafari, F. Ghanadi, and M. Arjomandi, Hinge and overturning moments due to unsteady heliostat pressure distributions in a turbulent atmospheric boundary layer. *Solar Energy*, 2019. 193: p. 604-617. doi: <https://doi.org/10.1016/j.solener.2019.09.097>

5. A. Jafari, F. Ghanadi, M. Arjomandi, M. J. Emes, and B. S. Cazzolato, Correlating turbulence intensity and length scale with the unsteady lift force on flat plates in an atmospheric boundary layer flow. *Journal of Wind Engineering and Industrial Aerodynamics*, 2019. 189: p. 218-230. doi: 10.1016/j.jweia.2019.03.029
6. A. Jafari, F. Ghanadi, M. J. Emes, M. Arjomandi, and B.S. Cazzolato, Effect of free-stream turbulence on the drag force on a flat plate, in 21st Australasian Fluid Mechanics Conference. 2018: Adelaide, Australia.
7. A. Pfahl, J. Coventry, M. Röger, F. Wolfertstetter, J. F. Vásquez-Arango, F. Gross, M. Arjomandi, P. Schwarzbözl, M. Geiger, and P. Liedke, Progress in heliostat development. *Solar Energy*, 2017. 152: p. 3-37.
8. B. Gong, Z. Li, Z. Wang, and Y. Wang, Wind-induced dynamic response of Heliostat. *Renewable Energy*, 2012. 38(1): p. 206-213. doi: <https://doi.org/10.1016/j.apm.2018.04.009>
9. D. T. Griffith, Adam C. Moya, Clifford K. Ho, and Patrick S. Hunter, Structural dynamics testing and analysis for design evaluation and monitoring of heliostats. *Journal of Solar Energy Engineering*, 2015. 137(2).
10. F. J. Vásquez-Arango, Reiner Buck, and Robert Pitz-Paal, Dynamic properties of a heliostat structure determined by numerical and experimental modal analysis. *Journal of Solar Energy Engineering*, 2015. 137(5): p. 051001-051001-5.
11. ESDU85020, Characteristics of atmospheric turbulence near the ground - Part II: single point data for strong winds (neutral atmosphere). Engineering Sciences Data Unit, 2010.
12. M. Emes, M. Marano, A. Jafari, and M. Arjomandi. Installation, Commissioning and Operation of the Atmospheric Boundary Layer Research Facility (ABLRF). in 23rd Australasian Fluid Mechanics Conference. 2022. Sydney, Australia.
13. M. Marano, M. Emes, A. Jafari, and M. Arjomandi. Heliostat Wind Load Field Measurements at the University of Adelaide Atmospheric Boundary Layer Research Facility (ABLRF). in SolarPACES. 2022. Albuquerque, New Mexico, USA.
14. G. S. Poulos, CASES-99: A comprehensive investigation of the stable nocturnal boundary layer. 2002. p. 555-581.
15. P. Drobinski, P. Carlotti, R. K. Newsom, R. M. Banta, R. C. Foster, and J. L. Redelsperger, The structure of the near-neutral atmospheric surface layer. *Journal of the Atmospheric Sciences*, 2004. 61(6): p. 699-714.
16. D. Krug, W.J., Baars, N., Hutchins, and I. Marusic. Vertical Coherence of Turbulence in the Atmospheric Surface Layer: Connecting the Hypotheses of Townsend and Davenport. *Boundary-Layer Meteorol* 172, 199–214 (2019).
17. A. Jafari, F. Ghanadi, M. J. Emes, M. Arjomandi, and B. S. Cazzolato, Measurement of unsteady wind loads in a wind tunnel: Scaling of turbulence spectra. *Journal of Wind Engineering and Industrial Aerodynamics*, 2019. 193: p. 103955. doi: <https://doi.org/10.1016/j.jweia.2019.103955>
18. R. Sankaran and E. D. Jancauskas, Direct measurement of the aerodynamic admittance of two-dimensional rectangular cylinders in smooth and turbulent flows. *Journal of Wind Engineering and Industrial Aerodynamics*, 1992. 41(1): p. 601-611. doi:10.1016/0167-6105(92)90469-Q
19. G. L. Larose and F. M. Livesey, Performance of streamlined bridge decks in relation to the aerodynamics of a flat plate. *Journal of Wind Engineering and Industrial Aerodynamics*, 1997. 69-71: p. 851-860.